Ethylcellulose nanoparticles as a new “in vitro” transfection tool for antisense oligonucleotide delivery

S.Leitner[2,1], S. Grijalvo[2,1], C. Solans[1,2], R. Eritja[1,2], M.J. García-Celma[3,2], G. Calderó[1]

[1]Institut de Química Avançada de Catalunya (IQAC-CSIC). Jordi Girona 18-26, 08034 Barcelona, Spain.

[2]Centro de Investigación Biomédica en Red en Bioingeniería, Biomateriales y Nanomedicina (CIBER-BBN), Barcelona, Spain

[3]Departament de Farmàcia i Tecnologia Farmacèutica i Fisicoquímica. Univ. de Barcelona. IN2UB. Unitat Associada d’I+D al CSIC- Av Joan XXIII, s/n, 08028 Barcelona, Spain

GRAPHICAL ABSTRACT

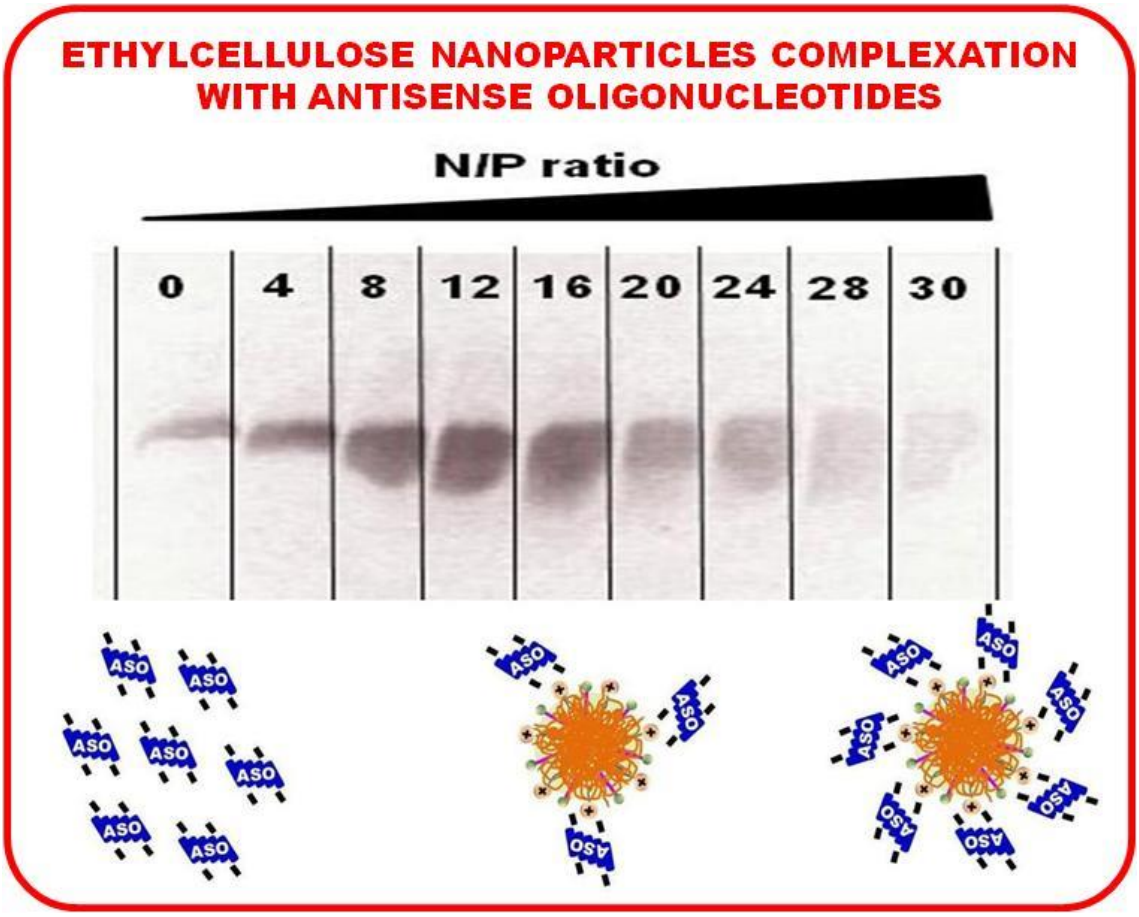

ABSTRACT

Oil-in-water nano-emulsions have been obtained in the HEPES 20 mM buffer solution / [Alkylamidoammonium:Kolliphor EL=1:1] / [6 weight % ethylcellulose in ethyl acetate] system over a wide oil-to-surfactant (O/S) range and above 35 weight% aqueous component at 25ºC. The nano-emulsion with an O/S ratio of 70/30 and 95 weight % aqueous component was used for nanoparticles preparation. These nanoparticles (mean diameter around 90 nm and zeta potential of +22 mV) were non-toxic to *HeLa* cells up to a concentration of 3 mM of cationic species. Successful complexation with an antisense phosphorothioate oligonucleotide targeting *Renilla* luciferase mRNA was achieved at cationic/anionic charge ratios above 16, as confirmed by zeta potential measurements and an electrophoretic mobility shift assay, provided that no Fetal Bovine Serum is present in the cell culture medium. Importantly, *Renilla* luciferase gene inhibition shows an optimum efficiency (40%) for the cationic/anionic ratio 28, which makes these complexes promising for “in vitro” cell transfection.

KEYWORDS

Ethylcellulose; nano-emulsion; nanoparticle; antisense oligonucleotide; “in vitro” transfection

ABBREVIATIONS LIST

ASO: Antisense oligonucleotide; CatA: Cationic amidoammonium amphiphile (ricinoleamidopropyltrimonium methosulfate); CEL: Kolliphor EL (also known as Cremophor®EL) ; DLS: Dynamic Light Scattering; DMEM: Dulbecco’s Modified Eagle’s Medium; EC10: Ethylcellulose; EMSA: Electrophoretic Mobility Shift Assay; FBS: Fetal Bovine Serum; FDA: Food and Drug Administration; g: grams; HEPES: 4-(2-Hydroxyethyl)piperazine-1-ethanesulfonic acid; HLB:

Hydrophilic-Lipophilic Balance; MTT : 3-(4,5- dimethylthiazol-2-yl)-2,5-diphenyltetrazolium bromide; mL: milliliter; mM: millimolar; mRNA: Messenger ribonucleic acid; mV: millivolts; MW: Molecular Weight; NE: Nano-emulsion; nM : Nanomolar; NP: Nanoparticle dispersion; N/P ratio : cationic-to-anionic charge ratio; O/S: Oil-to-surfactant ratio; PBS: Phosphate buffered saline; TBE: TRIS-Borate-EDTA buffer; W/O: Water-in-Oil; wt%: Weight percent; WT: Wild Type.

1. INTRODUCTION

Gene delivery is attracting increasing attention for the development of new therapeutic approaches such as the treatment of diseases considered until now incurable, and also for diagnostic purposes. However, nucleic acids are easily degradable by nucleases and their negative charge and often large size hinder their cellular uptake. Strategies to overcome low stability and poor cell penetration ability encompass both, the delivery through nanocarriers and the synthesis of short chain, chemically modified nucleic acid derivatives. Nanocarriers may contribute not only enhancing cell penetration but also allowing the condensation of the genetic material and its protection towards enzymatic degradation. Moreover, improved cell penetration is also favoured using shorter nucleic acid chains. In this context, oligonucleotides have been investigated in recent years, as they are short synthetic single stranded molecules, generally consisting of 13 to 25 nucleotides (Khvorova et al 2017). In particular, antisense oligonucleotides (ASOs) can be synthesized with sequences able to bind to specific mRNA strands preventing its translation into the proteins they encode, thus reducing, restoring or modifying their expression (Rinaldi et al. 2018). This has promoted research as new therapeutic tools against a large variety of genetic diseases, such as cystic fibrosis (Zamecnik et al. 2004), amyotrophic lateral sclerosis (Miller et al. 2013), β-thalassemia (Lacerra et al. 2000), familial hypercholesterolemia disease (Wong et al. 2014), inflammatory bowel diseases (Di Fusco et al. 2019), etc. Since 2016, five

oligonucleotides have been approved namely for the treatment of hepatic veno-occlusive disease, Duchenne muscular atrophy, spinal muscular atrophy and hereditary transthyretin amyloidosis (Yin et al. 2019). In addition, numerous oligonucleotide-based biosensors for *in vitro* diagnostics and environmental hazard detection are also being investigated as they are expected to impart fast, highly specific and sensitive detection (Jung et al. 2016; Platella et al. 2018). To increase their resistance to degradation by nucleases, several chemical modifications of the sugar ring, the nucleobases or the phosphate backbone have been proposed so far. Modification of the latter one is quite common and is often performed by replacing the phosphate group by a phosphorothioate group, consisting of a sulfur atom attached to the phosphate. This modification has been demonstrated to provide an increased stability to the oligonucleotide.

A challenging issue is the design of gene delivery vectors of non-viral origin. Although viral vectors are highly efficient, they may show safety concerns (immunogenicity, oncogenesis, etc.) and their production and shelf life is limited. Therefore, non-viral vectors are preferred (Mintzer et al 2009; Hall et al. 2017; Olden et al 2018). However, in spite of their higher loading capacity, they possess lower transfection efficiency than viral vectors, and the duration of gene expression is transient. Commercially available lipid-based transfection agents are frequently used as reference gene delivery vectors but some of them have been reported to have a negative impact on cell viability and are rather expensive (Mashal et al. 2017 and 2018; Yang et al. 2014). Therefore other alternative materials, like carbohydrate polymers have attracted attention, encompassing chitosan (Rahmani et al. 2019; Csaba et al. 2009; Nafee et al. 2007), amylopectin (Zhou et al. 2012), cationic dextran (Hu el al. 2019) or starch derivatives (Thiele et al. 2017). Nevertheless, to our best knowledge, ethylcellulose has not been investigated yet for nucleic acid transfection. The renewable resources origin, good biocompatibility, easy availability and low cost of this carbohydrate polymer encourage its use in this field. Ethylcellulose, is a hydrophobic semi-synthetic cellulose derivative, listed as “generally recognized as safe” and approved by the FDA for the oral, transdermal and transmucosal route at daily maximum allowable doses of 308 mg, 80 mg and 50 mg

respectively (FDA Inactive Ingredient Database; Arca et al. 2018). As a cellulose derivative, it consists on a linear chain of ß-anhydroglucose units linked through 1,4-glycosidic bonds. Although this backbone is common to other cellulose derivatives, like cellulose acetate or nitrocellulose, in ethylcellulose, the three free hydroxyl groups present in the anhydroglucose unit are partially substituted by ethoxyl groups. It is worth mentioning that the remaining free hydroxyls may form hydrogen bonds, favouring intra- and intermolecular interactions. This strongly influences the physical properties of the polymer and is exploited for example for the formation of oleogels as fat replacers in food industry (Aguilar-Zárate et al. 2019). Cellulose derivatives are used in a wide range of application fields, encompassing ceramics, printing inks, personal care products, food or pharmaceuticals, to mention a few. A current challenge in the pharmaceutical field is attaining nanosized structures, as this size range allows interactions at a subcellular level. Nanostructures of cellulose derivatives can be prepared both, by top-down and bottom-up techniques. Among top-down techniques, electrospinning allows attaining a large variety of complex structures which have demonstrated to be useful for the controlled release of drugs (Liu et al. 2018; Yang et al. 2019; Wang et al. 2017). As for bottom-up techniques, the low-energy emulsification approach is an environmentally friendly method, which has been reported for the preparation of ethylcellulose nanoparticles (Spernarth et al. 2007; Generalova et al. 2009; Calderó et al. 2011). Although ethylcellulose is nonionic, recently it has been shown that positively charged ethylcellulose nanoparticle dispersions can be obtained through nano-emulsion templating in cationic:non-ionic surfactant-based systems (Leitner et al. 2019; Calderó et al. 2019). These oil-in-water (O/W) nano-emulsion templates are obtained by a low-energy method and the positive surface charge of the dispersed systems is attributed to the cationic surfactant. The surfactant adsorbs at interfaces with the polar head group oriented towards the aqueous continuous phase of the nano-emulsion. Therefore, the cationic surfactant provides a positive surface charge to the nano-emulsion drops and the nanoparticles obtained from them. Positive surface charge provides ethylcellulose nanomaterials with new potential abilities such as improved mucoadhesivity, antibacterial properties or enhanced drug loading through electrostatic interactions.

The aim of this research work is to investigate for the first time the potential of positively charged ethylcellulose nanoparticles as antisense oligonucleotide carriers and transfection agents using a new cationic:non-ionc surfactant mixture for nano-emulsion templating, with the purpose of attaining optimum particle size and surface charges for “in vitro” gene delivery.

2. EXPERIMENTAL

2.1. Materials

Ethylcellulose, (**Figure 1a**) a commercial cellulose ether derivative, was from Colorcon, a distributor of the Dow Chemical Company (ETHOCEL™ Premium Std 10 ethylcellulose polymer, abbreviated as EC10. ETHOCEL is a trademark of the Dow Chemical Company). Ethoxyl content was 48.7% and the weight-average molecular weight (Mw) was 66385 ± 322 Dalton with a polydispersity of 4.3 as determined by Gel Permeation Chromatography (Leitner et al. 2019). Ethyl acetate (> 99.8%) was from Merck. The cationic amidoammonium amphiphile, ricinoleamidopropyltrimonium methosulfate (**Figure 1c**), in the following abbreviated as CatA, was from Evonik. It has an active matter content of 40 wt% in water and a critical micellar concentration of 3.3 x 10^{-2} mM (Burgos-Mármol et al. 2016). Kolliphor EL (also known as Cremophor®EL, from now on abbreviated as CEL) is a nonionic surfactant (HLB number of 12-14) manufactured by BASF (Cremophor EL Technical Information, BASF 2004; Kolliphor Grades. BASF Technical Sheet; Rowe et al. 2009). Water was deionized and MilliQ® filtered. HEPES salt (4-(2-Hydroxyethyl)piperazine-1-ethanesulfonic acid) was from Sigma Aldrich. It was used to prepare the HEPES 20 mM buffer which was adjusted at a pH of 7.4. An antisense phosphorothioate oligonucleotide (MW 5712 g/mol) of 18 nucleotides complementary to the mRNA of the *Renilla* luciferase gen, targeting the luciferase mRNA between positions 20 and 40” was purchased from Proligo (Sigma–Aldrich, **Figure 1b**). Lipofectamine 2000 was purchased from Invitrogen. Dulbecco's Modified Eagle's Medium (DMEM), heat-inactive fetal

serum bovine (FBS), TRIS-Borate-EDTA (TBE) buffer, PBS buffer, and distilled water (DNAse/RNAse free) were purchased from Gibco (Waltham, Massachusetts, USA). Luciferase assay kits were purchased from Promega (Madison, Wisconsin, USA).

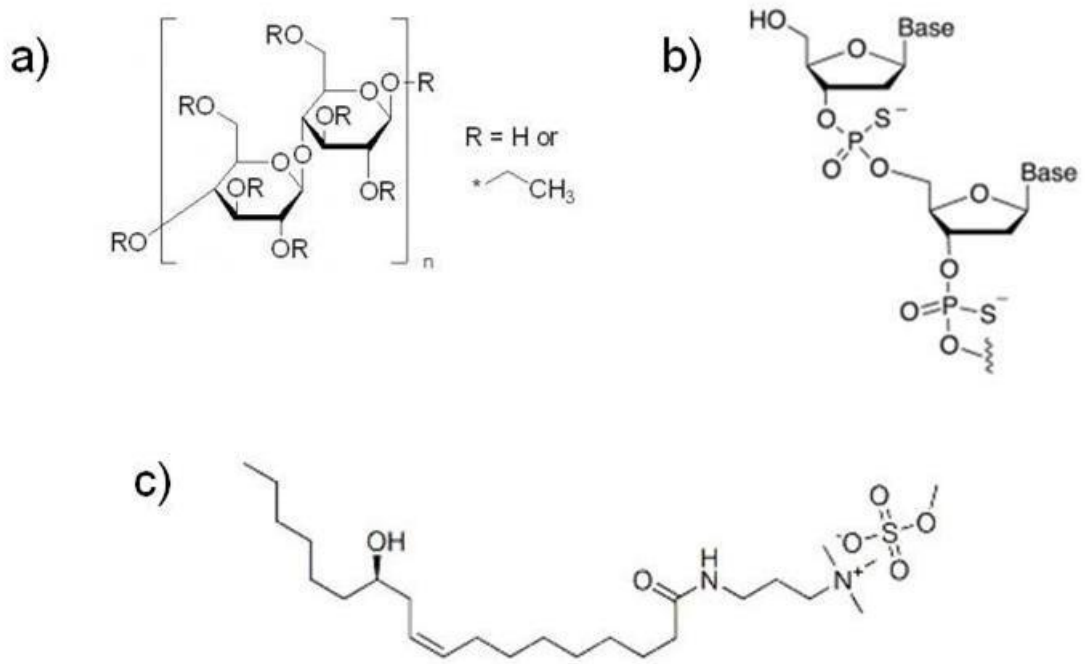

Figure 1: Chemical structure of a) Ethylcellulose polymer; b) Phosphorothioate oligonucleotide backbone; c) ricinoleamidopropyltrimonium methosulfate (CatA).

2.2. Methods

2.2.1. Preparation of oil-in-water (O/W) nano-emulsions

About 4 g of nano-emulsions were prepared in a 5 mL test tube, at a constant temperature of 25°C by adding HEPES buffer solution dropwise to the mixture of the oil (6 wt% of ethylcellulose in ethyl acetate) and mixed surfactants (Cat A:CEL = 1:1), which were previously homogenized. The addition of HEPES 20 mM buffer solution was performed under permanent vortex stirring (Vortex Genie 2^{TM}, Scientific Industries Inc.) at about 2700 rpm.

2.2.2. Nano-emulsion domain determination

The region of formation of O/W nano-emulsion in the HEPES 20 mM buffer solution / [CatA:CEL = 1:1] / [6 wt% EC10 in ethyl acetate] system was at first assessed visually at 25°C. Samples with various O/S ratios and HEPES contents were prepared as described in **Section 2.2.1**. Compositions with a translucent to transparent appearance and a reddish or bluish shine when observed through a lamp light were identified as nano-emulsions.

2.2.3. Phase Inversion determination

The phase inversion region was determined by conductivity measurements. Samples (2 g) were prepared by addition of HEPES 20 mM to oil/surfactant mixtures up to 95 wt%. Electrical conductivity of samples was measured at each composition by means of a Crison-GLP 31 conductimeter with a Pt/platinized electrode under continuous magnetic stirring at 25ºC.

2.2.4. Nanoparticle preparation

Nanoparticles were prepared by the solvent evaporation method using a rotary evaporator (Büchi) during 45 minutes under reduced pressure of 43 mbar and at 25°C. The condensator was set at -15ºC with the help of a low-temperature thermostat (Lauda RE-107 Ecoline Staredition). After evaporation, weight loss of the sample was replaced with Milli Q® water.

2.2.5. Nanoparticle:antisense nucleotide complex formation

Nanoparticle:antisense oligonucleotide (ASO) complexes were formed by adding increasing amounts of nanoparticles to a fixed concentration of ASO in order to attain the required cationic-to-anionic charge ratios, referred to as N/P ratios. This ratio is calculated as follows:

$$N/P = \frac{Number\ of\ equivalents\ of\ CatA}{Number\ of\ equivalents\ of\ oligonucleotide}$$

The resulting solutions are vortex mixed, then sonicated in a water bath for 5 minutes at 25ºC to facilitate complex formation and finally incubated at 37ºC for 40 minutes before characterization.

2.2.6. Particle size characterization

Dynamic light scattering: The mean size of nano-emulsions droplets and nanoparticles was determined with a 3D-DLS dynamic light scattering instrument (LS Instruments A. G., Switzerland) equipped with a He-Ne laser (λ=632.8 nm) and detection limit from 0.5 nm to 5 μm. Measurements were carried out in triplicate at a scattering angle of 90° and a temperature of 25 °C. The viscosity of the medium was taken as 0.889 cP. The refractive index of HEPES 20 mM was 1.334 as determined on an Abbe refractometer (Atago 3T, Japan) at 25ºC. DLS data were treated by cumulant analysis to obtain the hydrodynamic radius (Pecora et al. 2000; Brown 1993).

Transmission Electron Microscopy (TEM): Nanoparticle size was also determined by using the transmission electron microscope JEOL JEM 1010 (Jeol Korea Ltd.), operating at 80 kV. The samples were prepared just after solvent evaporation. A drop of the nanoparticle dispersion was placed on a carbon coated copper grid and then negatively stained with 2 wt% uranyl acetate (UA) solution. About 1000 particles were sized manually from about 50 TEM micrographs taken at different magnifications. For this purpose, the software package Image J was used. Data were evaluated with the Origin software package for particle size distribution calculation.

2.2.7. Shrinking factor determination

The shrinking factor upon nanoparticle formation from the nano-emulsion droplets was determined as the ratio between the volume of the template nano-emulsion droplet and the volume of the nanoparticle formed. For the calculation of the respective volumes, the mean hydrodynamic radii, as determined by DLS (see section 2.2.5.) are used.

$$f = \frac{V_{NE}}{V_{NP}} = \frac{{}^{4}/_{3}\ \pi\ r_{NE}^{3}}{{}^{4}/_{3}\ \pi\ r_{NP}^{3}} = \frac{r_{NE}^{3}}{r_{NP}^{3}}$$

where *f* is the shrinking factor; V_{NE} and V_{NP} are the volumes of a nano-emulsion drop and a nanoparticle respectively; r_{NE} and r_{NP} are the mean hydrodynamic radii or the nano-emulsion and the nanoparticle dispersion, as determined by DLS. Data are interpreted considering that no droplet size change due to coalescence, Ostwald ripening or flocculation occurs during solvent evaporation and that each single nano-emulsion drop generates one nanoparticle. A shrinking factor of 1 would mean no volume reduction of the template nano-emulsion droplet to form the nanoparticle, thus suggesting that no significant amount of ethyl acetate is present in the dispersed phase of the nano-emulsion.

2.2.8. Nano-emulsion and nanoparticle dispersion stability

Nano-emulsion and nanoparticle dispersion stability was assessed both, by visual observation of phase separation and by light scattering measurements over several weeks of samples stored at a controlled constant temperature of 25ºC. For the visual assessment, nano-emulsions and nanoparticle dispersions were considered stable when no macroscopic phases were observed.

2.2.9. Nano-emulsion and nanoparticle surface charge

The zeta potential, a measure of the net surface charge, was determined from the electrophoretic mobility measured by laser Doppler velocimetry using a ZetaSizer Nano Z laser diffractometer (Malvern Instruments), by applying the Smoluchowsky equation. For the measurements, nano-emulsions and nanoparticle dispersions were diluted with water to a concentration of 20 mg sample /g solution. Each sample was measured in triplicate at 25ºC.

2.2.10. Osmolality determination

Osmolality was measured on a freezing point osmometer (Micro-Osmometer Type 15, Löser Messtechnic), allowing measurements in the range from 0 to 2500 mOsm/Kg with a reproducibility of ±0.5%. For the measurements 100 µL of sample are required. Results are expressed in milliOsmols of solute per kilogram of solvent (mOsm/Kg).

2.2.11. Electrophoretic mobility shift assay

Electrophoretic Mobility Shift Assay (EMSA) was used to confirm successful complex formation between nanoparticles and oligonucleotides. Phosphorothioate antisense oligonucleotides (0.5 µg) were vortex mixed with increasing concentrations of the ethylcellulose nanoparticle dispersion in order to achieve positive to negative nanoparticle-to-oligonucleotide charge ratios (from now on referred as N/P ratio) between 0 and 30. Mixtures were subsequently incubated during 40 minutes at 37°C. The complexes were seeded on a 20 wt% polyacrylamide gel using TBE 1x as running buffer and subjected to electrophoresis at 150V for 8 hours. Shifts were visualized with a Gel Logic 200 imaging system after staining the gel with the fluorescent dye SYBR® Green (TBE 1x 200 mL; 20 µl) for 20 minutes under smooth shaking.

2.2.12. *In vitro* cytotoxicity determination

HeLa cells viability in the presence of nanoparticles at different concentrations was tested using a 3-(4,5- dimethylthiazol-2-yl)-2,5-diphenyltetrazolium bromide (MTT) assay. This is a colorimetric assay assessing mainly the mitochondrial activity. The water-soluble yellow MTT dye undergoes enzymatic reduction by the dehydrogenase system of alive cells giving rise to water insoluble purple formazan crystals. For each assay, about 7 x 10^3 cells/well were seeded on a 96-well plate in 100 µL Dulbecco's Modified Eagle's Medium (DMEM) and cultured for 24 hours. After complete adhesion to the plate, the culture medium was discarded. Nanoparticle dispersion was added at growing concentrations between 1.8 and 6.0 mM. The cells were incubated for 4 hours at 37ºC under 5% CO_2 atmosphere. Then, the nanoparticle dispersion was discarded and

DMEM (200 µL) was added. Cells were then further incubated for 15 hours at 37°C. MTT was added at a final concentration of 0.5 mg/mL per (25 µL) and was incubated for 2 hours at 37°C. Finally, the medium was removed and 200 µL DMSO per well were added to dissolve the purple formazan crystals formed. Absorbance was measured (Spectra Max M5 by Molecular Devices) at a wavelength of 570 nm, 30 min after the addition of DMSO. The cell viability was calculated as a percent ratio of the absorbance of cells treated with nanoparticle dispersion against the absorbance measured in untreated cells used as control. Results are expressed as the mean value of nine independent tests carried out for each concentration.

2.2.13. Transfection efficiency assay

HeLa cells were cultured at 37ºC, 5% CO_2 in DMEM partially supplemented with 10% fetal bovine serum (FBS), 100 µg/mL penicillin and 100 µg/mL streptomycin. Cells were regularly passaged to maintain exponential growth. 24 hours before transfection at 50 – 80% confluency, cells were trypsinized and diluted 1:5 with fresh medium without antibiotics (1-3 x 10^5 cells/mL) and transferred to 24-well plates (500 µL per well). Two luciferase plasmids, *Renilla* luciferase (pRL-TK) and *Firefly* luciferase (pGL3) from Promega, were used as reporter and control, respectively. *Renilla* and *Firefly* luciferase vectors (0.1 µg and 1.0 µg per well, respectively) were transfected into the cells using Lipofectamine 2000 (Invitrogen). Cells were incubated with the plasmids for 6 hours. Medium was discarded and the cells were washed with PBS. Then, 500 µL of fresh medium without antibiotics were added to each well. Two transfection experiments were carried out using either DMEM without FBS or DMEM supplemented with 10% of FBS. The antisense oligonucleotide was prepared at concentrations of 60, 150 and 270 nm. Nanoparticle:antisense oligonucleotide complexes which were incubated previously for 40 minutes at 37°C using HEPES (20 mM, pH 7.4) as buffer, were prepared at different concentrations. 100 µL of sample (naked antisense oligonucleotides (Wild Type, WT) or nanoparticle:antisense oligonucleotide complexes at the required concentrations) were added to each well. 22 hours after transfection cell lysates

were prepared and analyzed using the Dual-Luciferase Reporter Assay System according to the manufacturer's protocol. Luminiscence was measured using a SpectraMax M5 luminometer. As controls, a blank was prepared consisting on the cell culture transfected with the luciferase vectors in the absence of nanoparticles and antisense nucleotides and a Wild Type (WT) control, consisting on the transfected cell culture exposed to the antisense nucleotide in the absence of the ethylcellulose nanoparticle carrier. Results are calculated as the normalized ratios between the absorbance measured for the reporter pGL3 gene and the control pRL-TK luciferase gene, and are expressed as the mean and standard deviation of three independent experiments.

3. RESULTS AND DISCUSSION

3.1. Ethylcellulose nanoparticle preparation from nano-emulsion templates

Ethylcellulose nanoparticles have been obtained from nano-emulsion templates prepared by the phase inversion composition method. For this purpose, first the oil-in-water (O/W) nano-emulsion domain was determined in the HEPES 20 mM / [CatA:CEL = 1:1] / [6 wt% EC10 in ethyl acetate] system, at 25°C. HEPES 20 mM aqueous solution adjusted at a pH value of 7.4 was selected as the aqueous component for nano-emulsion preparation because it is a particularly suited buffer in cell culture and hence convenient for the purpose of the current research work (Ferguson et al. 1980). As shown in **Figure 2a**, nano-emulsions form in the oil-to-surfactant (O/S) range between 45/55 and 90/10, above 35 wt% HEPES 20 mM buffer solution content. At higher O/S ratios, the nano-emulsion region stretches to lower aqueous component contents, suggesting that O/S ratios between 70/30 and 85/15 favor the formation of nano-emulsions. The formation of the nano-emulsions through phase inversion was confirmed by

conductivity measurements performed along an experimental path with a constant O/S ratio (**Supplementary Information 1**). As shown in **Figure 2b**, the nano-emulsions formed display typically a translucent to transparent appearance, depending on the O/S ratio and the HEPES 20 mM content, with a bluish shine due to the Tyndall effect. This appearance is strikingly different from previously reported systems prepared with the same cationic surfactant (CatA) but different nonionic surfactants (namely Span 80 and Cremophor WO7) which showed higher opacity (Leitner et al 2019; Calderó et al 2019). It is also worth mentioning that in the system described herein, the nano-emulsion domain is considerably larger than in the latter mentioned systems.

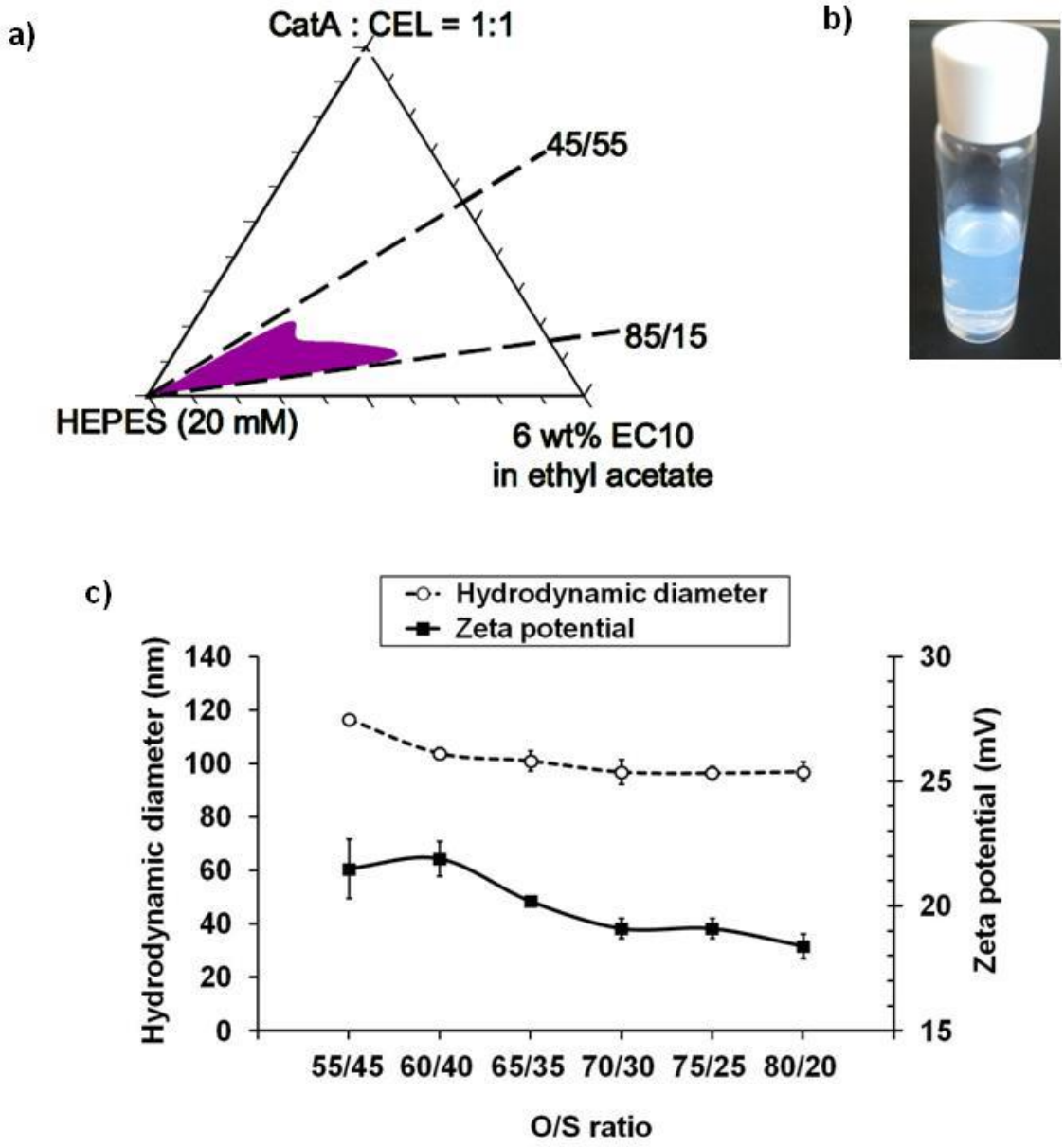

Figure 2: a) Oil-in-water (O/W) nano-emulsion domain (coloured area) in the HEPES 20 mM, pH=7.4 / [CatA:CEL= 1:1] / [6%EC10 in ethyl acetate] system at 25ºC; b) Visual appearance of the nano-emulsion with an O/S ratio of 70/30 and 95 wt% HEPES content; c) Hydrodynamic diameter (hollow circles) and zeta potential (filled squares) values of the nano-emulsions with varying oil-to-surfactant (O/S) ratios and a fixed 95 wt% HEPES 20 mM buffer solution content.

The nano-emulsions with a 95 wt% of HEPES 20 mM buffer solution content were selected for further characterization. As shown in **Figure 2c**, droplet size of the nano-emulsions did not vary significantly for oil-to-surfactant (O/S) ratios ranging between 60/40 and 80/20. These display mean diameters around 100 nm. However, at an O/S ratio of 55/45 the droplet diameter is somewhat larger (around 115 nm). All tested compositions show positive zeta potential values around 20 mV with a very slight tendency to decrease at increasing O/S ratios. Interestingly, positively charged ethylcellulose nano-emulsions obtained in similar systems with the same cationic surfactant but different nonionic surfactants show considerably larger droplet sizes. Thus, the nano-emulsion with an O/S ratio of 70/30 and 95 wt% water of the Water / [CatA: Cremophor WO7 = 1:1]/ [6% EC10 in ethyl acetate] system reported earlier showed a mean droplet size of around 195 nm and a zeta potential of about 47 mV, both larger than those of the current system (Calderó et al 2019). In that system, it was shown that the CatA:Cremophor WO7 ratio had a higher impact on the droplet size and the zeta potential of the nano-emulsions than the O/S ratio. Also, the nano-emulsion with the same O/S ratio of 70/30 but 90 wt% water of the Water / [CatA:Span80= 1:1] / [6% EC10 in ethyl acetate] system at 25ºC, showed a droplet size above 250 nm and a considerably higher zeta potential (around 55 mV) (Leitner et al 2019). These comparative data suggest that the nonionic surfactant used in the [CatA:nonionic surfactant] mixture plays a relevant role in the formation, droplet size and surface charge of the nano-emulsions. It is worth recalling that no nano-emulsions are formed with CatA in the absence of nonionic surfactant. In contrast, in systems containing only nonionic surfactant, ethylcellulose nano-emulsions can be formed (Calderó et al. 2011 and 2016).

This fact reinforces the idea of the crucial role of the nonionic surfactant in nano-emulsion formation. Nevertheless, the cationic surfactant is required for attaining a positive zeta potential, as in systems containing only the nonionic surfactant the zeta potential is negative, with values typically around –25 mV (Calderó et al. 2011 and 2016). Another important feature is the preparation method. Here, the phase inversion composition method is used. No nano-emulsions are formed if the components are mixed at once or following a different experimental path. Further, the aqueous component may also have an influence on the nano-emulsion characteristics. In particular, concerning the surface charge, the zwitterionic species present in the HEPES buffer solution might exert a neutralizing effect, lowering for that reason the zeta potential value.

The visual stability assessment of the nano-emulsion with an O/S ratio of 70/30 and 95 wt% HEPES (from now on designated as NE) revealed no macroscopic changes over one week at 25ºC. Further, droplet size remained unchanged for at least 3 weeks at the same storage temperature of 25ºC (**Figure 3a**). Therefore, considering the high stability of this nano-emulsion, as well as the suitable droplet sizes and zeta potential values (about +20 mV), it was selected for nanoparticles preparation by solvent evaporation. As expected, the nanoparticle dispersion shows a zeta potential value close to that of its nano-emulsion template, while the mean particle diameter is about 90.8 ± 1.4 nm as assessed by DLS. This size is smaller than that of the template nano-emulsion (96.9 ± 4.6 nm). As polydispersity indexes of both, the nano-emulsion and the nanoparticle dispersion are high (around 0.4), mean size data should be considered with caution. However, it should be taken into account that high polydispersity indexes are usual in dispersed systems prepared with preformed polymers. An interesting parameter is the calculated shrinking factor of the nano-emulsion for nanoparticle formation, which here is 1.9. This value is much higher than expected for a nano-emulsion with 95 wt% aqueous component. In earlier reported systems, the shrinking factor of nano-emulsions at this aqueous component content was close to 1, that is, the volume of the nanoparticle and that of the nano-emulsion drop were very similar (Calderó et al. 2019). The rather high shrinking factor in the current system suggests that the interfacial

film in this nano-emulsion might be more efficient in avoiding solvent diffusion from the dispersed drop to the continuous phase along the dilution path followed for its preparation, in spite of the more favorable osmotic gradient expected with HEPES 20 mM buffer solution as compared to water. In fact, the osmolality of deionized water is zero, while that of the HEPES 20 mM buffer solution at pH 7.4 used was 33 mOsm/Kg. The visual macroscopic stability of the nanoparticle dispersion is at least as high as that of the nano-emulsion template, and particle size remains stable for over 4 weeks when stored at 25ºC (**Figure 3a**). The nanoparticles obtained display a globular morphology, as observed by TEM after negative staining with uranyl acetate solution (**Figure 3b**). Particle size assessment by image analysis reveals a mean diameter of about 41 ± 10 nm, that is, roughly half the size measured by DLS. This is attributed to the fact that the measurements by DLS provide the size of the solvated particles, while by TEM image analysis the hard sphere size is measured. In addition, as already mentioned above, the zeta potential value of the nanoparticle dispersion is similar to that of the template nano-emulsion.

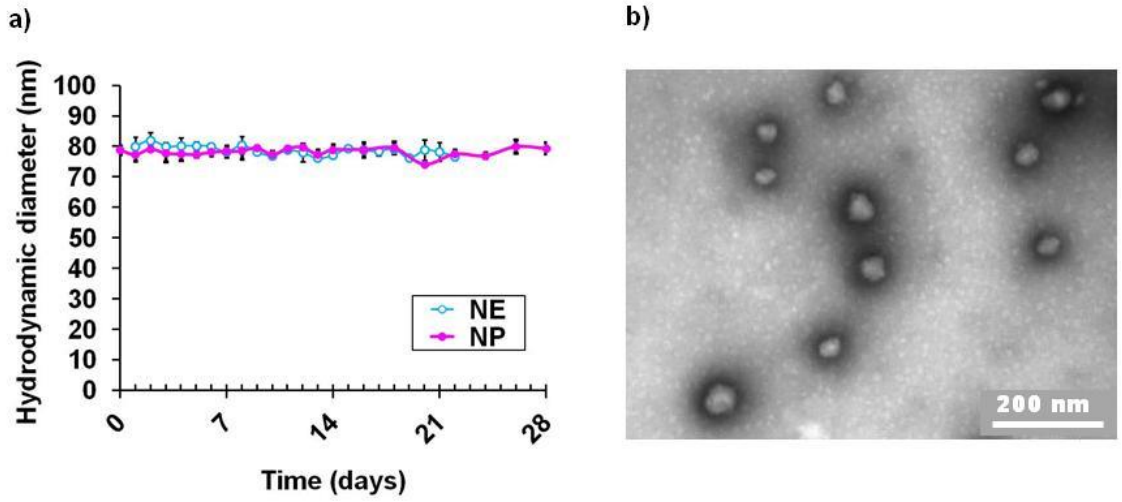

Figure 3: a) Particle size as measured by DLS as a function of time of the nano-emulsion (NE) of the HEPES 20 mM buffer solution / [CatA:CEL = 1:1] / [6 wt% EC10 in ethyl acetate] system with an O/S ratio of 70/30 and 95 wt% HEPES and the nanoparticle dispersion (NP) obtained from the nano-emulsion

at 25ºC; and b) TEM micrograph of the negatively stained nanoparticle dispersion.

3.2. Formation and characterization of ethylcellulose nanoparticles:oligonucleotide complexes

The formation of complexes of the positively charged ethylcellulose nanoparticles with an antisense oligonucleotide (ASO) was studied. The ASO are negatively charged due to the presence of phosphorothioate groups in the molecule backbone (**Figure 1b**). Increasing amounts of nanoparticle dispersion were added to a fixed concentration of ASO, as explained in detail in the experimental section, in order to attain cationic (nanoparticles)-to-anionic (ASO) charge ratios (N/P) ranging from 0 to 30. As shown in **Figure 4a**, the nanoparticles:ASO complex size kept roughly constant around 90 nm, regardless the N/P ratio. In the absence of ASO, the nanoparticles show a mean size of 90.8 nm as measured by DLS and a zeta potential value of +22.0 mV. Although it might be expected that complex size is larger than the bare nanoparticles, this is not observed here. This might be explained by a compaction due to electrostatic interaction, and may also be considered as a sign that no instability by aggregation has occurred (Li et al. 2011; Puras et al. 2014; Rahmani et al. 2019). It is also worth mentioning that the size range, which is below 200 nm, is within that reported as appropriate for cell membrane penetration (Davis *et al.* 2009; Yasar et al. 2018).

Zeta potential values are negative when the naked oligonucleotide (without the nanoparticles) is present (N/P ratio 0, about -15 mV), which is due to the negative phosphate groups in the backbone of the oligonucleotide. Surface charge values remain in this range up to N/P ratio 8. At N/P ratios ≥ 8, a pronounced increase to almost neutral zeta potential values takes place. This behavior is generally recognized as an indication of electrostatic interactions

between the negatively charged species and the positively charged nanoparticles (Ogris et al. 1999; Putnam et al. 2001; Davis et al. 2009; Hartl et al. 2019). At N/P ratios ≥ 16, surface charge values reach a plateau (neutral or slightly negative values). At these N/P ratios it is assumed that full complexation is achieved. Although the long-term stability of the nanoparticles:ASO complexes has not been determined, these did not show signs of instability during the experimental time. Stability may be favoured by their small size (hydrodynamic diameters around 90 nm, as determined by DLS).

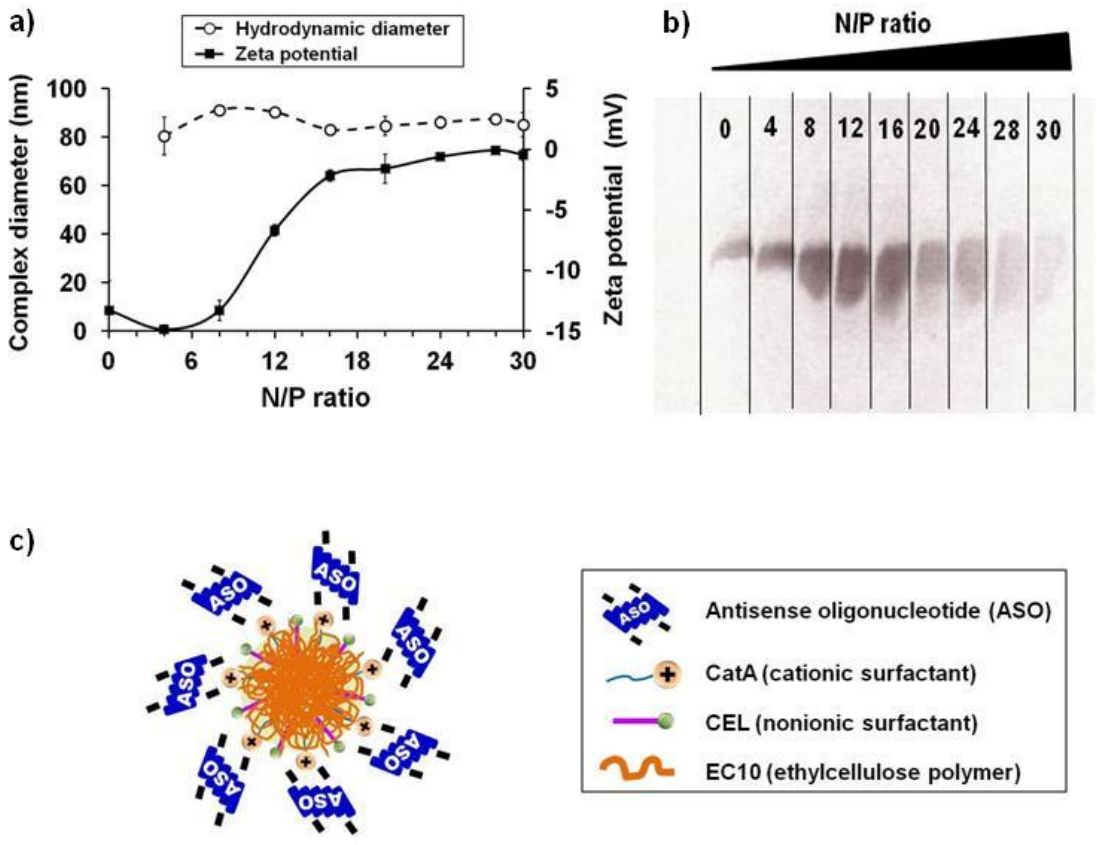

Figure 4: a) Size (empty circles) and zeta potential (black squares) values as a function of the N/P ratio of complexes formed between nanoparticles and the antisense oligonucleotide (ASO) phosphorothioate, at 25°C; **b)** EMSA gel shift assay obtained after 8 hours, to analyse the ability of the nanoparticles to form complexes with the antisense oligonucleotide (ASO) phosphorothioate. The

mobility of ASO is retarded upon complexation causing the fading away of the band of stained ASO in the polyacrylamide gel at increasing N/P ratio, indicating successful nanoparticles:ASO complex formation; **c)** Schematic illustration of a nanoparticle:ASO complex. Nanoparticles were obtained from nano-emulsions of the HEPES solution / CatA:CEL = 1:1] / [6 wt% EC10 in ethyl acetate] system with an O/S ratio of 70/30 and 95 wt% HEPES solution

The surface charge of the complexes was also measured in the presence of Fetal Bovine Serum (FBS) which is frequently used in transfection studies, as an approach to physiological conditions encountered in “in vivo” environments. It is well known that in biological media nanoparticles undergo a coating process mainly by adsorption of proteins forming a layer designated as “protein corona”. This protein corona endows nanoparticles with a new biological identity which determines its physiological impact, such as immune response and hence blood clearance rate, biodistribution, cell penetration, interaction with receptors, etc. (Monopoli et al. 2012). As illustrated in the **Supplementary Information 2**, in the presence of FBS, nanoparticle:ASO complexes displayed a negative zeta potential at all N/P charge ratios studied. Zeta potential values are more negative when oligonucleotide and serum without nanoparticles are present (N/P ratio 0, about -25 mV) as additional negative charges coming from serum proteins are present. Surface charge values increase up to -15 mV for N/P ratio 8 and then only slightly for N/P ratios > 8, staying in the negative range (about -10 mV). These results suggest that negatively charged components in serum were, depending on the charge ratio, presumably adsorbed onto the surface of the nanoparticle complexes. Similar results are reported by Li *et al.* (Li et al. 2011), who found that the zeta potential values of liposome/DNA complexes (lipoplexes) in the absence of serum were positive and increased with increasing N/P ratio. In the presence of serum, however, lipoplexes displayed negative zeta potential values at all studied N/P ratios which was attributed to negatively charged components in serum adsorbed onto the surface of the lipoplex particles. Interestingly, other studies carried out by

means of zeta potential isotherms on the adsorption of bovine serum albumin (BSA) onto differently functionalized PLGA nanoparticles revealed that upon saturation of the nanoparticle surface with BSA, the zeta potential value remained constant at approximately – 10 mV (Fornaguera et al. 2015). This suggests that the constant value around -10 mV attained here regardless the N/P ratio may be attributed to complex surface saturation with serum proteins. It is also worth recalling that albumin is the main protein in serum.

To further confirm the complex formation between nanoparticles and ASO, electrophoretic mobility shift assays (EMSA) were performed. This experiment was carried out without FBS and as described in **Section 2.2.11**. **Figure 4b** shows the results obtained. The mobility of ASO in the polyacrylamide gel is retarded upon complexation with the nanoparticles, which is detected by a shift and fading away of the band of the stained ASO at increasing N/P ratio, indicating successful nanoparticles:ASO complex formation The numbers between the vertical lines in the figure indicate the N/P ratio. The negative control is designated 0, i.e. it contains only ASO. With increasing N/P ratio, the band gets broader which was assumed to be due to the formation of complexes with different sizes (polydispersity). For the N/P ratio 20 the band is less intense than for smaller N/P ratios and the higher the N/P ratio is, the more fades the band. The fading of the band is interpreted as a sign of complex formation and retardation (Lundberg et al. 2007). These EMSA results are in good agreement with those obtained from surface charge measurements (**Figure 6a**), both suggesting that complex formation is achieved at N/P ratios ≥ 16. This N/P ratio is comparable to that reported for other gene delivery systems (Lee et al. 2016).

Figure 5 shows a TEM micrograph obtained from the nanoparticle:ASO complex with an N/P ratio of 30, the highest studied N/P ratio in which complexation took place. Complexes showed a rounded shape, similar to that observed for pristine nanoparticles, and have a mean size of 30 nm (by TEM image analysis). This value differs significantly from that obtained by DLS (about 90 nm). As mentioned previously, the sizes measured from TEM micrographs correspond to the hard sphere sizes while DLS provides sizes of the solvated complexes. Also the high polydispersity (>0.4 by DLS) has to be taken into account. **Figure 5b** compares the size distributions of the

583 nanoparticle dispersion and the nanoparticle:ASO complex. Both size
584 distributions are monomodal. The main population of the bare nanoparticle
585 dispersion is at 40 nm and is shifted towards smaller sizes when the complex
586 with ASO is formed. This decrease in mean size has to be taken with caution as
587 the polydispersity in both systems is rather high. However, it should be also
588 considered that electrostatic interactions may favour the compaction of the
589 structure, thus yielding smaller entities.

590

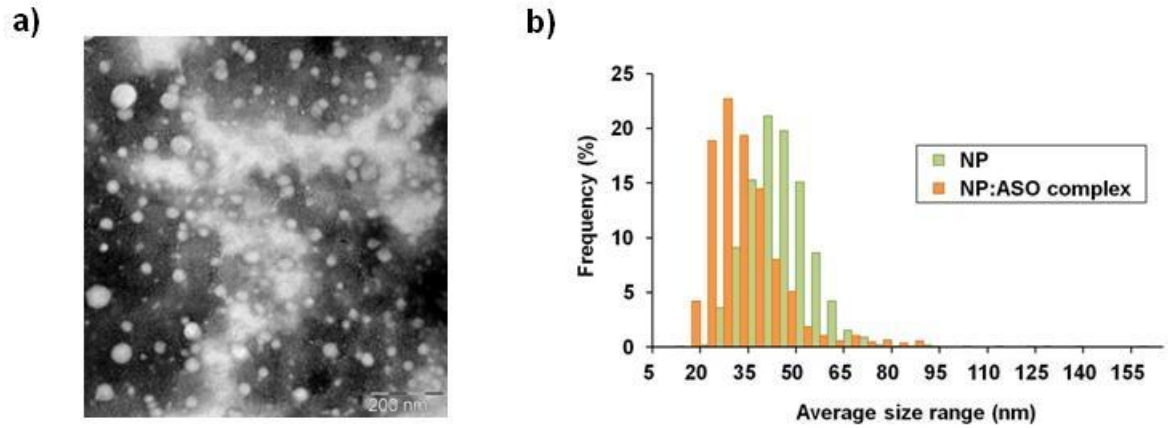

591

592 **Figure 5: a)** TEM micrograph of the negatively stained complex between the
593 nanoparticle dispersion and the antisense oligonucleotide phosphorothioate, at
594 the N/P ratio 30. Nanoparticles were obtained from a nano-emulsion of the
595 HEPES 20 mM solution / [CatA:CEL = 1:1] / [6wt% EC10 in ethyl acetate]
596 system with an O/S ratio of 70/30 and 95 wt% HEPES solution; **b)** Complex size
597 distributions, assessed from TEM image analysis, of a negatively stained
598 nanoparticle dispersion and of the complex between nanoparticles and the
599 antisense oligonucleotide phosphorothioate, at the N/P ratio 30. Nanoparticles
600 were obtained from nano-emulsions of the HEPES solution / CatA:CEL = 1:1] /
601 [6 wt% EC10 in ethyl acetate] system with an O/S ratio of 70/30 and 95 wt%
602 HEPES solution

603

604

605 **3.3. Biological characterization**

The nanoparticle dispersion of the HEPES 20 mM solution / [CatA:CEL = 1:1] / [6 wt% EC10 in ethyl acetate] system with an O/S ratio of 70/30 and 95 wt% HEPES solution selected for the complexation studies was further investigated to determine its toxicity and transfection efficiency.

3.3.1. Cytotoxicity assessment by the MTT assay

The viability and proliferation of HeLa cells in the presence of nanoparticles was evaluated by performing the MTT cytotoxicity assay on HeLa cells. The studies were carried out as described in **Section 2.2.12**. The absorbance of the colored complex solutions was measured at a wavelength of 570 nm and graphically represented as a function of cationic species concentration present in CatA (40 wt% of active matter), as shown in **Figure 6**. Keeping in mind that cell viability is directly proportional to the amount of formazan produced by the enzymatic activity of living cells, the measured absorbance gives an idea of the number of viable cells when compared with the control (i.e. here cells in the absence of nanoparticles).

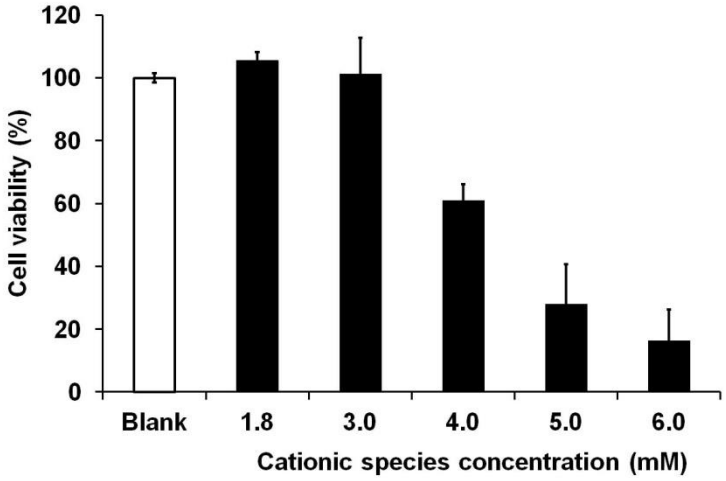

Figure 6: Cell viability (%) of HeLa cells as a function of nanoparticle concentration after 4 hours of treatment. The **blank** bar indicates the sample without nanoparticles.

The graphic shows that cell viability decreases slightly at 3 mM with respect to the blank while at higher concentration it is considerably reduced, indicating that no cytotoxicity occurs up to a concentration of 3 mM, referred to the cationic species. It is well known that generally, cytotoxicity increases with increasing cationic charge. The behavior displayed by our positively charged nanoparticles is in good agreement with other studies carried out with cationic nanoparticles, which showed increased cytotoxicity with increasing concentration of cationic polymer (Putnam et al 2001).

3.3.2. Transfection efficiency of nanoparticle:oligonucleotide complexes

The ability of the cationic nanoparticles to form complexes with the antisense oligonucleotide (ASO) phosphorothioate through electrostatic interactions has been described and proved in the previous sections. As mentioned, the ASO chosen for our study inhibits the *Renilla* luciferase gene. The transfection efficiency of the nanoparticles:ASO complexes in the absence and presence of Fetal Bovine Serum (FBS) has been evaluated. At first, the optimal ratio between the antisense oligonucleotide and the nanoparticles was determined. For this purpose, cells were cotransfected with two luciferase plasmids (*Renilla* and *Firefly*; target and internal control, respectively). Then both, the naked antisense oligonucleotide designed to inhibit the expression of *Renilla* luciferase gene as well as the nanoparticle:ASO complexes were added to the transfected cells in the presence and absence of fetal bovine serum. After 24 hours incubation, the luciferase activities of the samples were measured by using a luminometer. **Figure 7a** plots the *Renilla* luciferase activity normalized to *Firefly* luciferase as a function of the nanoparticle to ASO charge ratio (N/P), keeping a constant ASO concentration of 60 nM in the absence of serum. As inferred from the zeta potential values and the electrophoretic mobility shift assay shown before, formation of nanoparticle:ASO complexes took place at N/P ratios equal to or above 16 (**Figure 4a**). As full complexation was assumed in the plateau range of zeta potential, which was confirmed by gel shift assays (**Figure 4b**), two N/P ratios of the plateau range (N/P 28 and 30) were selected for

transfection assays and a N/P ratio higher than those studied (N/P 35) in order to study the influence of higher complex ratios. It is worth mentioning that several authors have reported the ability of some antisense oligonucleotides to penetrate into the cells through their membrane without the help of transfection agents, by a process called gymnosis (Stein et al. 2010; Moschos et al. 2011 ; Martirosyan 2018). Nevertheless, previous reported experiments have discarded this cell entry capability for the ASO studied here (Fornaguera et al. 2015b; Mayr et al. 2017). In addition, as shown in **Figures 7a and 7b**, the luciferase activity of the transfected HeLa cells in the absence (Blank) and the presence of the antisense oligonucleotide (Wild Type) were similar and close to unity. This result confirms that the oligonucleotide alone is not able to reach the cytoplasm of the HeLa cells to inhibit the expression of the *Renilla* luciferase gene. However, it was found that the nanoparticles:ASO complexes were able to transfect the antisense oligonucleotide as the expression of *Renilla* luciferase gene was specifically inhibited. The highest inhibitory properties were found with nanoparticle:antisense oligonucleotide complexes at the charge ratio of N/P 28 obtaining around 40% inhibition efficiency in serum-free medium. Reported values of *Renilla* luciferase silencing in HeLa cells by Lipofectamine 2000 (frequently used as a positive control reference) are around 84% for at an ASO concentration of 60 nM, and below 60% for cationic surfactant vesicles at ASO concentrations above 60 nM (Grijalvo et al. 2014; Mayr et al. 2017). The inhibition efficiency of our nanoparticle:antisense oligonucleotide complex is similar to that of dendronized poly(lactic-co-glycolic) acid nanoparticles functionalized with third generation cationic dendrons (around 40% inhibition) and higher than that of nanoparticles functionalized with second generation cationic dendrons (about 20% inhibition) at the same 60 nM ASO concentration, although for these both carriers the N/P ratio is much lower (0.75/1) due to the high positive charge density on the dendron distal surface (Fornaguera et al. 2015b).

Surprisingly, higher N/P ratios in our nanoparticle:ASO complexes did not provide improved transfection efficiency. Thus, N/P charge ratios of 30 only produced a knockdown value of about 11%. This might be attributed to a stronger binding of the ASO to the positively charged nanoparticle, hence

reducing the release of the ASO. Several authors have reported that an optimum balance between nucleic acid complexation and release from their carrier is required for an efficient transfection (Pacharoenchai et al. 2012; Puras et al. 2014). It is also worth noticing that the luciferase activity at the N/P ratio of 35 exceeded that of the blank and the naked ASO (WT). This effect has been described in other non-viral vectors, such as proline-rich cell-penetrating peptides (Grijalvo et al. 2012), dendronized PLGA nanoparticles (Fornaguera et al. 2015b) or cationic vesicles (Mayr et al. 2017). Although in our study the complex size did not vary significantly in the N/P range studied, complex aggregation phenomena in the cellular environment may not be ruled out, thus hindering their penetration into the cell, as pointed out by several authors (Xiong et al. 2011; Mayr et al. 2017). For this reason, the N/P ratio of 28 was considered to be the optimal for transfecting antisense oligonucleotides with these nanoparticles:ASO complexes in the experimental conditions tested.

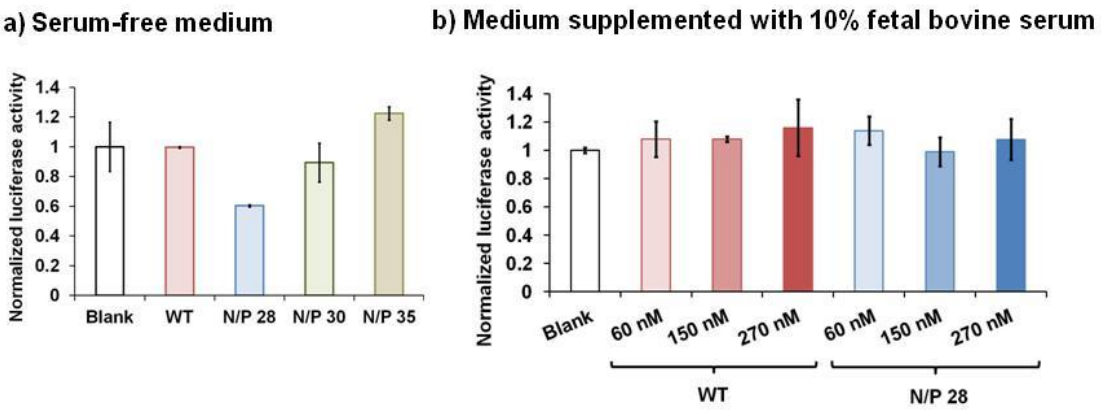

Figure 7: **a)** Gene-specific silencing activities for phosphorothioate antisense oligonucleotide, targeting the *Renilla* luciferase mRNA expressed in HeLa cells. a) In serum-free medium. The N/P (nanoparticle:antisense oligonucleotide) ratios tested for gene knockdown were N/P 28, 30 and 35. The ASO concentration was 60 nM. **b)** In medium supplemented with 10% serum for unmodified phosphorothioate antisense oligonucleotide (**WT**) at different concentrations (60, 150 and 270 nM) and for the nanoparticle:ASO complexes at N/P ratio 28 (nanoparticle:antisense oligonucleotide) using mentioned ASO concentrations. The bar named **Blank** is the result of luciferase activity of the HeLa cells with the two transfected plasmids. The bar named **WT** is the result without using nanoparticles.

In addition the transfection of HeLa cells was also tested in cell culture media supplemented with fetal bovine serum. This allows simulating more closely physiological conditions, with the aim to assessing the possibility of being used *in vivo*, where high concentrations of numerous proteins are encountered. For this study, the N/P charge ratio of the complex was set at 28 as it was judged to be the optimal for transfection in the absence of serum. In addition, ASO concentrations above 60 nM (namely 150 and 270 nM) were also tested. As shown is **Figure 7b**, the normalized luciferase activity was around 1 for all tested samples, which implies that no gene silencing was detected in the presence of serum. Several factors may account for the lack of inhibition of the luciferase expression, such as the coating of the complex with serum proteins, the displacement of the ASO by serum proteins and lipoproteins, thus reducing or even completely quenching the ASO binding to the positively charged nanoparticles or the increased electrostatic interactions between the nanoparticles:ASO complexes and serum components giving rise to large aggregates unable to penetrate into the cells. These transfection efficiency results in the presence of FBS preclude the use of these nanoparticles:ASO complexes for *in vivo* experiments. However, they can be used for gene inhibition in cell cultures.

4. CONCLUSIONS

Positively charged ethylcellulose nano-emulsions have been obtained in the HEPES 20 mM buffer solution / [CatA:CEL = 1:1] / [6 wt% EC10 in ethyl acetate] system. These nano-emulsions as well as the nanoparticles obtained from them show smaller sizes than those described earlier in similar systems. The nanoparticles have a convenient biocompatibility profile and in spite of their moderate positive surface charge (around + 20 mV), successful complexation with an antisense oligonucleotide (ASO) has been achieved. *In vitro* transfection

tests revealed that although in the presence of serum no gene silencing was detected, optimum transfection efficiency (40%) was achieved at N/P ratio 28 in serum-free medium. These results encourage further research on the use of these complexes for *in vitro* diagnostic tests as well as *in vivo* gene therapy using administration routes in which the impact of the adhesion of proteins present in the medium is expected to be lower than in the parenteral environment, such as the dermal or inner ear route of administration.

5. CONFLICTS OF INTEREST

The authors declare no conflict of interests.

6. ACKNOWLEDGEMENTS

The DLS, zeta potential and Turbiscan analyses have been performed at the Nanostructured Liquid Characterization Unit, located at the Institute of Advanced Chemistry of Catalonia (IQAC), belonging to the Spanish National Research Council (CSIC) and affiliated to the NANBIOSIS ICTS of the Biomedical Networking Center (CIBER-BBN). CIBER-BBN is an initiative funded by the VI National R&D&I Plan 2008-2011. Financial support from MINECO (grant CTQ2017-84998-P (AEI/FEDER,UE) and Generalitat de Catalunya (grant 2009SGR-961) is acknowledged. S.L. is grateful to CIBER-BBN for a research scholarship. Colorcon and Bonderalia S.A./Quimivita S.A. and BASF are gratefully acknowledged for the gift of ethylcellulose, ricinoleamidopropyltrimonium methosulfate and Kolliphor EL respectively.

7. REFERENCES

777 Aguilar-Zárate M, Macias-Rodriguez BA, Toro-Vazquez JF, Marangoni AG.
778 Engineering rheological properties of edible oleogels with ethylcellulose
779 and lecithin. Carbohydrate Polymers 2019; 205: 98–105

780 Arca HC, Mosquera-Giraldo LI, Bi L, Xu D, Taylor LS, Edgar KJ.
781 Pharmaceutical applications of cellulose ethers and cellulose ether
782 esters. Biomacromolecules 2018; 19: 2351-2376

783 Brown W., Dynamic Light Scattering: The Method and Some Applications,
784 Oxford University Press, New York, 1993.

785 Burgos-Mármol JJ, Solans C, Patti A. Effective short-range Coulomb correction
786 to model the aggregation behaviour of ionic surfactants. J Chem Phys
787 2016; 144: 234904 DOI 10.1063/1.4954063

788 Calderó C., García-Celma M.J., Solans C., Formation of polymeric nano-
789 emulsions by a low-energy method and their use for nanoparticle
790 preparation. Journal of Colloid and Interface Science 2011; 353: 406-
791 411

792 Calderó G., Montes R., Llinàs M., García-Celma M.J., Porras M., Solans C.
793 Studies on the formation of polymeric nano-emulsions obtained via low-
794 energy emulsification and their use as templates for drug delivery
795 nanoparticle dispersions. Colloids and Surfaces B: Biointerfaces 2016;
796 145: 922 – 931 DOI 10.1016/j.colsurfb.2016.06.013.

797 Calderó G, Leitner S, García-Celma MJ and Solans C. Modulating size and
798 surface charge of ethylcellulose nanoparticles through the use of cationic
799 nano-emulsion templates. Carbohydrate Polymers 2019. In press.

800 Cremophor EL Technical Information BASF. Solubiliser and emulsifying agent
801 for the human and veterinary pharmaceutical industries; used in aqueous
802 preparations of hydrophobic substances, e. g. fat-soluble vitamins and
803 essential oils. MEMP 030711e-03/Page 1 of 8. September 2004.

804 Csaba N, Köping-Höggård M, Fernandez-Megia E, Novoa-Carballal R, Riguera
805 R, Alonso MJ. Ionically crosslinked chitosan nanoparticles as gene

delivery systems: effect of PEGylation degree on in vitro and in vivo gene transfer. J Biomed Nanotechnology 2009; 5: 162–71

Davis ME. The First Targeted Delivery of siRNA in Humans via a Self-Assembling, Cyclodextrin Polymer-Based Nanoparticle: From Concept to Clinic. Molecular Pharmaceutics 2009; 6 (3): 659 – 668

Di Fusco D, Dinallo V, Marafini I, Figliuzzi MM, Romano B, Monteleone G. Antisense Oligonucleotide: Basic Concepts and Therapeutic Application in Inflammatory Bowel Disease. Front. Pharmacol. 2019; 10:305-312. doi: 10.3389/fphar.2019.00305

Ferguson WJ, Braunschweiger KI, Braunschweiger WR, Smith JR, McCormick JJ, Wasmann CC, Jarvis NP, Bell DH, Good NE. Hydrogen ion buffers for biological research. Analytical Biochemistry 1980; 104 (2): 300-310

FDA Inactive Ingredient Database for Approved Drug Products, https://www.fda.gov/drugs/informationondrugs/ucm113978.htm

Fornaguera et al. 2015 a. Fornaguera C, Calderó G, Mitjans M, Vinardell MP, Solans C, Vauthier Ch. Interactions of PLGA nanoparticles with blood components: protein adsorption, coagulation, activation of the complement system and hemolysis studies. Nanoscale 2015; 7: 6045-6058

Fornaguera et al. 2015 b. Fornaguera C, Grijalvo S, Galán M, Fuentes-Paniagua E,, de la Mata FJ, Gómez R, Eritja R, Calderó G, Solans C. Novel non-viral gene delivery systems composed of carbosilane dendron functionalized nanoparticles prepared from nano-emulsions as non-viral carriers for antisense oligonucleotides. International Journal of Pharmaceutics 478 (2015) 113–123

Generalova AN, Sizova SV, Oleinikov VA, Zubov VP, Artemyev MV, Spernath L, Kamyshny A, Magdassi S. Highly fluorescent ethyl cellulose nanoparticles containing embedded semiconductor nanocrystals. Colloids and Surfaces A: Physicochemical and Engineering Aspects 2009; 342(1-3): 59-64

836 Grijalvo, S.; Eritja, R. Synthesis and in vitro inhibition properties of
837 oligonucleotide conjugates carrying amphipathic proline-rich peptide
838 derivatives of the sweet arrow peptide (SAP). Mol. Div. 2012, 16, 307–
839 317

840 Hall A, Lächelt U, Bartek J, Wagner E, Moghimi SM. Polyplex Evolution:
841 Understanding Biology,Optimizing Performance. Molecular Therapy
842 2017; 25 (7): 1476 - 1490

843 Hartl N, Adams F, Costabile G, Isert L, Döblinger M, Xiao X, Liu R, Merkel OM.
844 The Impact of Nylon-3 Copolymer Composition on the Efficiency of
845 siRNA Delivery to Glioblastoma Cells. Nanomaterials 2019; 9: 986-1013.
846 doi:10.3390/nano9070986

847 Hu Y, Wang H, Song H, Young M, Fan Y, Xu FJ, Qu X, Lei X, Liu Y, Cheng G.
848 Peptide-grafted dextran vectors for efficient and high-loading gene
849 delivery. Biomater. Sci. 2019; 7: 1543-1553

850 Jung IY, Lee EH, Suh AY, Lee SJ, Lee H. Oligonucleotide-based biosensors for
851 in vitro diagnostics and environmental hazard detection. Anal Bioanal
852 Chem 2016: 408: 2383-2406

853 Khvorova A, Watts JK. The chemical evolution of oligonucleotide therapies of
854 clinical utility. Nature Biotechnology 2017; 35 (3): 238-248

855 Kolliphor® Grades. Emulsifier for topical pharmaceutical applications. Technical
856 data sheet.2014 BASF 03_120610e-01/Page 1 of 6 WF-No. 125032

857 Lacerra G, Sierakowska H, Carestia C, Fucharoen S, Summerton J, Weller D,
858 Kole R. Restoration of hemoglobin A synthesis in erythroid cells from
859 peripheral blood of thalassemic patients. Proc Natl Acad Sci USA 2000;
860 97 (17): 9591-9596

861 Lee D-J, He D, Kessel E, Padari K, Kempter S, Lächelt U, Rädler JO, Pooga
862 M, Wagner E. Tumoral gene silencing by receptor-targeted combinatorial
863 siRNA polyplexes. Journal of Controlled Release 2016; 244: 280–291

Leitner S, Solans C, García-Celma MJ, Calderó G. Low-energy nano-emulsification approach as a simple strategy to prepare positively charged ethylcellulose nanoparticles. Carbohydrate Polymers 2019; 205: 117–124

Li L, Song H, Luo K, He B, Nie Y, Yang Y, Wu Y, Gu Z. Gene transfer efficacies of serum-resistant amino acids-based cationic lipids: Dependence on headgroup, lipoplex stability and cellular uptake. Int J Pharm. 2011 ; 408 (1-2): 183-90. doi: 10.1016/j.ijpharm.2011.01.051

Liu X, Shao W, Luo M, Bian J, Yu D-G. Electrospun Blank Nanocoating for Improved Sustained Release Profiles from Medicated Gliadin Nanofibers. Nanomaterials 2018, 8, 184; doi:10.3390/nano8040184

Lundberg P, El-Andaloussi S, Sütlü T, Johansson H, Langel Ü. Delivery of short interfering RNA using endosololytic cell-penetrating peptides. FASEB Journal 2007; 21 (11): 2664-2671

Martirosyan M, Olesen MJ, Fenton RA, Kjems J, Howard KA. Mucin-mediated nanocarrier disassembly for triggered uptake of oligonucleotides as a delivery strategy for the potential treatment of mucosal tumours. Nanoscale, 2016, 8, 12599

Mashal M, Attia N, Puras G, Martínez-Navarrete G, Fernández E, Pedraz JL. Retinal gene delivery enhancement by lycopene incorporation into cationic niosomes based on DOTMA and polysorbate 60. Journal of Controlled Release 2017; 254: 55–64

Mashal M, Attia N, Soto-Sánchez C, Martínez-Navarrete G, Fernández E, Puras G, Pedraz JL. Non-viral vectors based on cationic niosames as efficient gene delivery vehicles to central nervous system cells into the brain. International Journal of Pharmaceutics 2018; 552: 48-55

Mayr J, Grijalvo S, Bachl J, Pons R, Eritja R, Díaz Díaz D. Transfection of Antisense Oligonucleotides Mediated by Cationic Vesicles Based on Non-Ionic Surfactant and Polycations Bearing Quaternary Ammonium

Moieties. Int. J. Mol. Sci. 2017, 18, 1139 - 1142; doi:10.3390/ijms18061139

Miller TM, Pestronk A, David W, Rothstein J, Simpson E, Appel SH, Andres PL, Mahoney K, Allred P, Alexander K, Ostrow LW, Schoenfeld D, Macklin EA, Norris DA, Manousakis G, Crisp M, Smith R, Bennett CF, Bishop KM, Cudkowicz ME. An antisense oligonucleotide against SOD1 delivered intrathecally for patients with SOD1 familial amyotrophic lateral sclerosis: a phase 1, randomised, first-in-man study. Lancet Neurol. 2013 ; 12 (5) :435-42

Mintzer MA, Simanek EE. Nonviral Vectors for Gene Delivery. Chemical Reviews, 2009; 109 (2): 259-302

Monopoli MP, Åberg Ch, Salvati A, Dawson KA. Biomolecular coronas provide the biological identity of nanosized materials. Nature Nanotechnology 2012; 7: 779-786

Moschos SA, Frick M, Taylor B, Turnpenny P, Graves H, Spink KG, Brady K, Lamb D, Collins D, Rockel ThD, Weber M, Lazari O, Perez-Tosar L, Fancy SA, Lapthorn Ch, Green MX, Evans S, Selby M, Jones G, Jones L, Kearney S, Mechiche H, Gikunju D, Subramanian R, Uhlmann E, Jurk M, Vollmer J, Ciaramella G, Yeadon M. Uptake, Efficacy, and Systemic Distribution of Naked, Inhaled Short Interfering RNA (siRNA) and Locked Nucleic Acid (LNA) Antisense. Molecular Therapy 2011; 19 (12): 2163–2168

Nafee N, Taetz S, Schneider M, Schaefer UF, Lehr CM. Chitosan-coated PLGA nanoparticles for DNA/RNA delivery: effect of the formulation parameters on complexation and transfection of antisense oligonucleotides. Nanomedicine. 2007; (3):173-83

Ogris M, Brunner S, Schüller S, Kircheis R, Wagner E. PEGylated DNA/transferrin-PEI complexes: Reduced interaction with blood components, extended circulation in blood and potential for systemic gene delivery. Gene Therapy 1999; 6 (4): 595-605

923 Olden BR, Cheng Y, Yu JL, Pun SH. Cationic polymers for non-viral gene
924 delivery to human T cells. Journal of Controlled Release 2018; 282:140–
925 147

926 Paecharoenchai O, Niyomtham N, Ngawhirunpat T, Rojanarata T,
927 Yingyongnarongkul BE, Opanasopit P. Cationic niosomes composed of
928 sperminebased cationic lipids mediate high gene transfection efficiency.
929 J. Drug Target. 2012; 20 (9): 783–792.

930 Pecora R. Dynamic light scattering measurement of nanometer particles in
931 liquids. J Nanopart Res 2000; 2: 123–131 http://dx.doi.org/10.1023/
932 A:1010067107182.

933 Platella Ch, Musumeci D, Arciello A, Doria F, Freccero M, Randazzo A, Amato
934 J, Pagano B, Montesarchio D. Controlled Pore Glass-based
935 oligonucleotide affinity support: towards High Throughput Screening
936 methods for the identification of conformation-selective G-quadruplex
937 ligands. Analytica Chimica Acta 2018; 1030: 133e141

938 Puras G, Mashal M, Zárate J, Agirre M, Ojeda E, Grijalvo S, Eritja R, Diaz-
939 Tahoces A, Martínez Navarrete G, Avilés-trigueros M, Fernández E,
940 Pedraz JL. A novel cationic niosome formulation for gene delivery to the
941 retina. Journal of Controlled release 2014; 174: 27-36

942 Putnam D, Gentry CA, Pack DW, Langer R. Polymer-based gene delivery with
943 low cytotoxicity by a unique balance of side-chain termini. Proc Natl Acad
944 Sci U S A 2001; 98(3) :1200-1205

945 Rahmani S, Hakimi S, Esmaeily A, Samadi FY, Mortazavian E, Nazari M,
946 Mohammadi Z, Tehrani NR, Tehrani MR. Novel chitosan based
947 nanoparticles as gene delivery systems to cancerous and noncancerous
948 cells. International Journal of Pharmaceutics 2019; 560: 306–314

949 Rinaldi C, Wood MJA. Antisense oligonucleotides: the next frontier for treatment
950 of neurological disorders. Nature Reviews Neurology 2018; 14: 9–21

951 Rowe RC, Sheskey PJ, Quinn ME, Handbook of Pharmaceutical Excipients,
952 Pharm. Press, 6th edition 2009, pp. 542–549.

953 Spernarth L., Magdassi S. Preparation of ethyl cellulose nanoparticles from
954 nano-emulsion obtained by inversion at constant temperature. Micro and
955 Nano Letters 2007; 2(4): 90-95

956 Stein CA, Bo Hansen J, Lai J, Wu SJ, Voskresenskiy A, Høg A, Worm J,
957 Hedtjärn M, Souleimanian N, Miller P, Soifer HS, Castanotto D,
958 Benimetskaya L, Ørum H, Koch T. Efficient gene silencing by delivery of
959 locked nucleic acid antisense oligonucleotides, unassisted by
960 transfection reagents. Nucleic Acids Research, 2010, Vol. 38, No. 1 e3.
961 doi:10.1093/nar/gkp841

962 Thiele C, Loretz B, Lehr CM. Biodegradable starch derivatives with tunable
963 charge density-synthesis, characterization, and transfection efficiency.
964 Drug Deliv. and Transl. Res. 2017; 7:252–258

965 Wang Q, Yu DG, Zhang L-L, Liu X-K, Deng Y-Ch, Zhao M. Electrospun
966 hypromellose-based hydrophilic composites for rapid dissolution of poorly
967 water-soluble drug. Carbohydrate Polymers 2017; 174: 617–625

968 Wong E, Goldberg T. Mipomersen (Kynamro): a novel antisense oligonucleotide
969 inhibitor for the management of homozygous familial
970 hypercholesterolemia. Pharm Ther 2014; 39(2): 119-122

971 Xiong, F.; Mi, Z.; Gu, N. Cationic liposomes as gene delivery system:
972 Transfection efficiency and new application. Pharmazie 2011, 66, 158–
973 164.

974 Yang Y, Li W, Yu D-G, Wang G, Williams GR, Zhang Z. Tunable drug release
975 from nanofibers coated with blank cellulose acetate layers fabricated
976 using tri-axial electrospinning. Carbohydrate Polymers 2019; 203: 228–
977 237

978 Yang Z, Jiang Z, Cao Z, Zhang Ch, Gao D, Luo X, Zhang X, Luo H, Jiang Q,
979 Liu J. Multifunctional non-viral gene vectors with enhanced stability,
980 improved cellular and nuclear uptake capability, and increased
981 transfection efficiency. Nanoscale 2014; 6: 10193

Yasar H, Duy-Khiet Ho D-K, De Rossi Ch, Herrmann J, Gordon S , Loretz B, Lehr CM. Starch-Chitosan Polyplexes: A Versatile Carrier System for Anti-Infectives and Gene Delivery. Polymers 2018, 10, 252; doi:10.3390/polym10030252

Yin W, Rogge M. Targeting RNA: A transformative therapeutic strategy. Clin Transl Sci 2019; 12: 98-112

Zamecnik PC, Raychowdhury MK, Tabatadze DR, Cantiello HFReversal of cystic fibrosis phenotype in a cultured Delta508 cystic fibrosis transmembrane conductance regulator cell line by oligonucleotide insertion. Proc Natl Acad Sci USA 2004; 25; 101(21): 8150-5

Zhou Y, Yang B, Ren X, Liu Z, Deng Z, Chen L, Deng Y, Zhang LM, Yang L. Hyperbranched cationic amylopectin derivatives for gene delivery. Biomaterials. 2012; 33(18): 4731-40

SUPPLEMENTARY INFORMATION

Supplementary Information 1

Conductivity as a function of total aqueous solution content in the HEPES 20 mM / [CaA:CEL = 1:1] / [6 wt% EC10 in ethyl acetate] system along the dilution path with the O/S ratio of 70/30 at 25ºC.

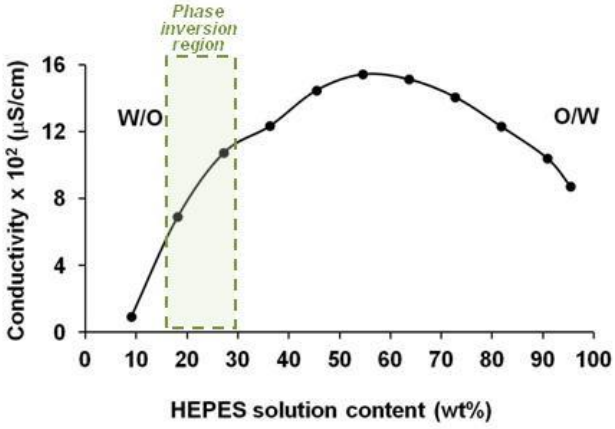

As shown, the conductivity values increase at increasing aqueous solution content and reach a maximum, which in this system is produced at about 1500 µS/cm. Then conductivity values gradually decrease due to the effect of dilution of the conducting species. It is worth mentioning that HEPES solution contains zwitterionic molecules. The conductivity values attained, as well as the conductivity variation as a function of the aqueous component content are comparable to those obtained with similar systems described earlier, containing the same cationic surfactant but different nonionic surfactants, namely Span 80 (Leitner et al. 2019) and Cremophor WO7 (Calderó et al. 2019). Phase inversion takes place at about 25 wt% HEPES solution.

Supplementary Information 2

Zeta potential values as a function of the N/P ratio of complexes formed between nanoparticles and the antisense oligonucleotide (ASO)

phosphorothioate in the presence of Fetal Bovine Serum (FBS), at 25°C. Nanoparticles were obtained from nano-emulsions of the HEPES solution / [CatA:CEL = 1:1] / [6 wt% EC10 in ethyl acetate] system with an O/S ratio of 70/30 and 95 wt% HEPES solution.